Genes & Nutrition

RESEARCH

Open Access

miR-450a-2-3p targets ERK(1/2) to ameliorate ISO-induced cardiac fibrosis in mice

Langsha Liu[1] and Fanyan Luo[2*]

Abstract

Objective Cardiac fibrosis is an important contributor to atrial fibrillation (AF). Our aim was to identify biomarkers for AF using bioinformatics methods and explore the regulatory mechanism of miR-450a-2-3p in cardiac fibrosis in mice.

Methods Two datasets, GSE115574 and GSE79768, were obtained from the Gene Expression Omnibus (GEO) database and subsequently merged for further analysis. Differential gene expression analysis was performed to identify differentially expressed genes (DEGs) and miR-450a-2-3p-related differentially expressed genes (MRDEGs). To investigate the underlying mechanism of cardiac fibrosis, a mouse model was established by treating mice with isoproterenol (ISO) and the miR-450a-2-3p agomir.

Results A total of 127 DEGs and 31 MRDEGs were identified and subjected to Gene Ontology (GO) functional enrichment analysis and Kyoto Encyclopedia of Genes and Genomes (KEGG) pathway enrichment analysis to determine the functions and pathways involved in AF. In the animal model, histological analysis using HE and Masson staining, as well as quantification of the collagen volume fraction (CVF), was performed. The increased expression of α-smooth muscle actin (α-SMA), collagen type I (COL1), collagen type III (COL3), and extracellular signal-regulated kinase 1/2 (ERK(1/2)) at both the transcriptional and translational levels indicated the significant development of myocardial fibrosis in mice induced with isoproterenol (ISO). In addition, the cross-sectional area of cardiomyocytes and the expression of atrial natriuretic peptide (NPPA) and brain natriuretic peptide (NPPB) were increased in the ISO group compared with the control group. However, after overexpression of the miR-450a-2-3p agomir through caudal vein injection, there was a notable improvement in cardiac morphology in the treated group. The expression levels of α-SMA, COL1, COL3, ERK(1/2), NPPA, and NPPB were also significantly decreased.

Conclusion Our study reveals the mechanistic connection between ISO-induced myocardial fibrosis and the miR-450a-2-3p/ERK(1/2) signaling pathway, highlighting its role in the development of cardiac fibrosis. Modulating miR-450a-2-3p expression and inhibiting ERK(1/2) activation are promising approaches for therapeutic intervention in patients with AF.

Keywords Atrial fibrillation, Cardiac fibrosis, MicroRNA, Mice

*Correspondence:
Fanyan Luo
xyyylfy@163.com
Full list of author information is available at the end of the article

Introduction

Atrial fibrillation (AF) is one of the most prevalent sustained supraventricular arrhythmias and is associated with an increased risk of stroke [1]. The underlying mechanism is believed to involve electrical and structural remodeling of the atria, leading to the development of cardiac fibrosis [2]. Cardiac fibrosis plays an important role in the persistence of AF and is considered one of the key factors contributing to its resistance to rhythm control interventions [3]. The activation and proliferation of cardiac fibroblasts (CFs), which are responsible for the excessive production of extracellular matrix (ECM) components such as c collagen type I (COL1) and collagen type III (COL3), play a crucial role in fibrogenesis in patients with AF [4]. Additionally, CFs can differentiate into myofibroblasts, cells that exhibit a twofold greater capacity for collagen synthesis and are characterized by alpha smooth muscle actin (α-SMA) expression [5]. Similarly, in cardiac fibrosis, endothelial cells (ECs) can undergo endothelial–mesenchymal transition (EndMT), acquiring a mesenchymal phenotype and expressing characteristic markers of myofibroblast differentiation, including α-SMA, vimentin, and collagens [6]. The expression of α-SMA, a well-characterized cytoskeletal protein, is a hallmark of myofibroblast differentiation [7]. However, the precise molecular mechanisms underlying cardiac fibrosis and EndMT in the setting of AF remain largely unclear.

In our previous study, we observed downregulation of miR-450a-2-3p in CFs and human umbilical vein endothelial cells (HUVECs) exposed to transforming growth factor (TGF)-β1, suggesting the potential of miR-450a-2-3p as a microRNA (miRNA) that inhibits cardiac fibrosis [8]. In the present study, we employed established bioinformatic tools to investigate the underlying mechanism of miR-450a-2-3p in cardiac fibrosis. Two transcriptome datasets were selected from the Gene Expression Omnibus (GEO) database for analysis. Differential gene expression analysis was conducted to identify differentially expressed genes (DEGs), as well as miR-450a-2-3p-related DEGs (MRDEGs). Subsequently, functional enrichment analysis revealed the involvement of miR-450a-2-3p in multiple biological processes and signaling pathways related to cardiac fibrosis. Furthermore, we validated the antifibrotic effect of miR-450a-2-3p overexpression in a mouse model of isoproterenol (ISO)-induced myocardial fibrosis. Collectively, our findings identify a previously unknown microRNA with potential utility as a target for future clinical treatment and diagnosis of AF patients.

Materials and methods

Ethics statement

This study was approved by the Ethics Committee of Central South University. This study was implemented in accordance with the Declaration of Helsinki. All animal experiments complied with the rules and regulations of experimental animal management and operating standards as well as the ethical requirements for the use of experimental animals. Additionally, all animal procedures were performed according to the standards of humane animal care approved by the Medical Ethics Committee of Central South University.

Data collection and downloading

The AF gene expression datasets GSE115574 and GSE79768 were obtained from the GEO database (https://www.ncbi.nlm.nih.gov/geo/). In GSE115574 (14 AF samples and 16 sinus rhythm (SR) samples), the patient numbers (AF) included AF01L, AF02L, AF03L, AF04L, AF05L, AF06L, AF07L, AF08L, AF09L, AF10L, AF11L, AF12L, AF13L, and AF14R. The control group numbers (SR) were SR01L, SR02L, SR03L, SR04L, SR05L, SR06L, SR07L, SR08L, SR09L, SR10L, SR11L, SR12L, SR13L, SR14L, SR15L, and SR16R. Specifically for the study, AF14R and SR16R representing the right atrial group and AF01L, AF02L, AF03L, AF04L, AF05L, AF06L, AF07L, AF08L, AF09L, AF10L, AF11L, AF12L, AF13L, SR01L, SR02L, SR03L, SR04L, SR05L, SR06L, SR07L, SR08L, SR09L, SR10L, SR11L, SR12L, SR13L, SR14L, and SR15L representing the left atrial group were used in the study. For GSE79768 (14 AF samples and 12 SR samples), patients (AF) with identifiers Atrial Fibrillation_ 14, Atrial Fibrillation_ 19, Atrial Fibrillation_ 20, Atrial Fibrillation_ 29, Atrial Fibrillation_ 32, Atrial Fibrillation_ 33, Atrial Fibrillation_ 34 were included. The control group (SR) identifiers were Sinus Rhythm_ 15, Sinus Rhythm_ 22, Sinus Rhythm_ 39, Sinus Rhythm_ 42, Sinus Rhythm_ 76, and Sinus Rhythm_ 92. Both left atrial and right atrial data were utilized in this study. The GSE115574 and GSE79768 datasets were generated using the GPL570 [HG-U133_Plus_2] Affymetrix Human Genome U133 Plus 2.0 Array platform. The R software packages "limma" and "SVA" were used to merge the GSE115574 and GSE79768 datasets, and batch effects were removed using the "combat" function. The p values were adjusted using the FDR method. Differentially expressed genes (DEGs) were identified in the merged dataset using the criteria $|\log FC| \geq 0.5$ and adj.P. Val. Filter < 0.05. The "heatmap" package and "ggplot2" package were utilized to generate heatmaps and volcano plots,

respectively, of the DEGs. Prediction of miRNA–mRNA interactions was performed using TargetScan (https://www.targetscan.org/vert_72/). 2.3 Functional enrichment analysis.

To investigate the roles of the DEGs in AF patients, we utilized the Xiantao online tool (https://www.xiantaozi.com/) to conduct GO functional enrichment and KEGG pathway enrichment analyses. Additionally, the Metascape database (http://metascape.org) was used to facilitate a comprehensive understanding of the biological significance of the MRDEGs through Gene Ontology enrichment analysis.

Mouse model of ISO-induced cardiac fibrosis and grouping

Eight-week-old male C57BL/6 mice were utilized to establish a cardiac fibrosis model through ISO induction. A total of 24 mice were randomly divided into four groups: the control group, ISO-induced model group, miR-450a-2-3p agomir group, and agomir-negative control (NC) group ($n=6$ mice per group). In the ISO-induced model and control groups, ISO (0.1 ml/10 g) and normal saline, respectively, were injected into the abdominal cavity of each mouse for 14 days. During this period, the mice were weighed on Days 1, 7, and 14. After the 14-day treatment period, the mouse whole heart tissues were collected for hematoxylin–eosin (HE) staining, Masson staining, Reverse transcription-quantitative polymerase chain reaction (RT-qPCR), and Western blot analysis. Each group consisted of 6 samples. The mice in the miR-450a-2-3p agomir and agomir-NC groups received injections of the miR-450a-2-3p agomir (5 nmol/mouse) and agomir-NC (5 nmol/mouse), respectively, with a total of four injections over a period of 16 days (once every 5 days). The miR-450a-2-3p agomir and agomir-NC (GenePharma, Shanghai, China) were administered via tail vein injection.

HE staining and masson staining

Paraffin-embedded heart tissue sections were dried in a 60 °C incubator for more than 3 h prior to staining. Standard protocols were followed for HE staining and Masson staining. The slides were examined using an optical microscope, and images were acquired to evaluate histopathological features and the extent of fibrosis. Images were acquired at a magnification of 400×. Each group consisted of 6 samples, and 4 regions were randomly selected from each sample, in which the cross-sectional area of cardiomyocytes was counted by ImageJ. Using image analysis software (Image-Pro Plus 6.0), semiquantitative analysis of the collagen-positive and collagen-negative areas was performed by adjusting the grayscale values. Through this analysis, the collagen volume fraction (CVF), which represents the ratio of the collagen area to the total area of the field of view, was determined.

RT-qPCR

Total RNA was extracted according to the manufacturer's instructions. Briefly, approximately 0.02 g of heart tissue was mixed well with 1 mL of TRIzol (Thermo Fisher Scientific, MA, USA) for 5 min. mRNA was reverse transcribed to cDNA using a reverse transcription kit (Cwbiotech, Beijing, China). RT–qPCR was performed using an UltraSYBR mixture (Cwbiotech, Beijing, China). The relative expression of genes was calculated using the $2^{-\Delta\Delta CT}$ method. The mmu-miR-450a-2-3p, COL1, COL3, atrial natriuretic peptide (NPPA), and brain natriuretic peptide (NPPB) expression level in each sample was normalized to that of GAPDH, and the α-SMA and ERK(1/2) expression level in each sample was normalized to that of U6. All primers used in this study were commercially obtained from Sangon (Shanghai, China) and are listed in Supplementary Table 1.

Western blot analysis

Mouse heart tissues (0.025 g) were lysed in 300 μL of RIPA buffer (Abiowell, Changsha, China). After centrifugation at 12,000×g for 15 min at 4 °C, the supernatant was collected. The protein concentration was determined using a bicinchoninic acid assay performed with a commercial kit (Cwbiotech, Beijing, China). Next, 120 μL of protein was separated using 5×loading buffer (30 μL) and then transferred to a nitrocellulose filter membrane. The membrane was incubated in 5% bovine serum albumin (BSA) at 4 °C for 1.5 h and then incubated with primary antibodies at 4 °C overnight. The primary antibodies used for Western blotting were as follows: anti-β-actin (1:5000; Proteintech, IL, USA), anti-α-SMA (1:3000; Proteintech, IL, USA), anti-COL1 (1:2000; Proteintech, IL, USA), anti-COL3 (1:500; Proteintech, IL, USA), and anti-ERK(1/2) (1:10,000; Proteintech, IL, USA). After overnight incubation with the primary antibodies, the membrane was incubated with the corresponding secondary antibodies (HRP goat anti-mouse IgG, 1:5000; HRP goat anti-rabbit IgG, 1:6000; Proteintech, IL, USA) at 25 °C for 90 min. Detection was performed using an enhanced chemiluminescence (ECL) system (Abiowell, Changsha, China). Relative protein expression levels were determined using Quantity One v4.6.2 software.

Statistical analysis

Two-tailed Student's t test was used for comparisons between two distinct conditions. When the data did not exhibit a normal distribution, the Mann–Whitney U test was utilized. For comparisons among three or more experimental groups, one-way ANOVA with Dunnett's post hoc test or Tukey's multiple comparison test was used. Statistical analysis was performed using GraphPad

Prism 8.0 software (GraphPad Software, San Diego, CA, USA). $P<0.05$ was considered to indicate statistical significance.

Results

Screening for DEGs in AF

The schematic flowchart of this study is presented in Fig. 1. Differential expression analysis was performed with 28 samples of atrial tissue from patients with AF and 28 samples of atrial tissue from patients with sinus rhythm (SR) represented in the GSE79768 and GSE115574 datasets. The box plots (Fig. 2A-B) and PCA plots (Fig. 2C) effectively demonstrated the successful elimination of batch effects between GSE79768 and GSE115574. In the merged expression matrix, 126 differentially expressed genes (DEGs), namely, 50 upregulated genes and 76 downregulated genes, were identified using the "limma" R package. The heatmap and volcano plot of the DEGs are shown in Fig. 3 for the comparison between AF and SR in the merged data cohort.

Functional enrichment analysis of DEGs and MRDEGs

To explore the potential functions of the DEGs, functional enrichment analysis of the DEGs was conducted based on GO terms and KEGG pathways. The various GO terms and KEGG pathways are presented in Fig. 4A and included muscle tissue development, gland morphogenesis, and morphogenesis of an epithelial fold in the biological process (BP) category; collagen-containing extracellular matrix, sarcomere, and myofibril in the cellular component (CC) category; extracellular matrix structural constituent, heparin binding, and glycosaminoglycan binding in the molecular function (MF) category; and the KEGG pathways aldosterone synthesis and secretion and PI3K-Akt signaling pathway. These results indicate strong correlations between the selected DEGs and cardiac fibrosis, suggesting that these DEGs play a crucial role in the development of AF.

Our previous study revealed that the overexpression of miR-450a-2-3p suppressed the expression of ERK(1/2) in cardiac fibroblasts (CFs), leading to the inhibition of α-SMA, COL1, and COL3 expression and the prevention of CF proliferation. In HUVECs, overexpression of miR-450a-2-3p upregulated the expression of VE-Cadherin (VE-Cad) and platelet endothelial cell adhesion molecule-1 (PECAM-1/CD31) by inhibiting the expression of ERK(1/2), while the expression levels of vimentin, COL1, and COL3 were decreased. Furthermore, we confirmed that ERK(1/2) is a direct target of miR-450a-2-3p using a luciferase assay.

Next, we aimed to further explore the relationships between the target genes of miR-450a-2-3p and the DEGs. The potential target genes of miR-450a-2-3p were predicted using TargetScan, a database for miRNA–target interactions, with 4893 target genes predicted. Subsequently, the miR-450a-2-3p-related differentially expressed genes (MRDEGs) that overlapped with the predicted miR-450a-2-3p target genes and the DEGs were identified. Finally, 31 significant MRDEGs were selected using the overlap between the two datasets, as indicated

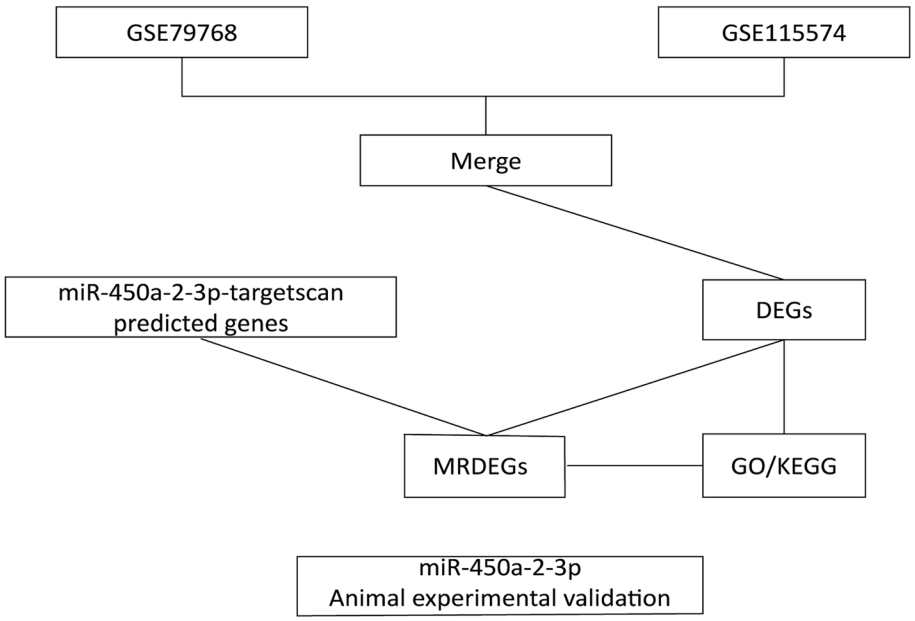

Fig. 1 The overall protocol for this study

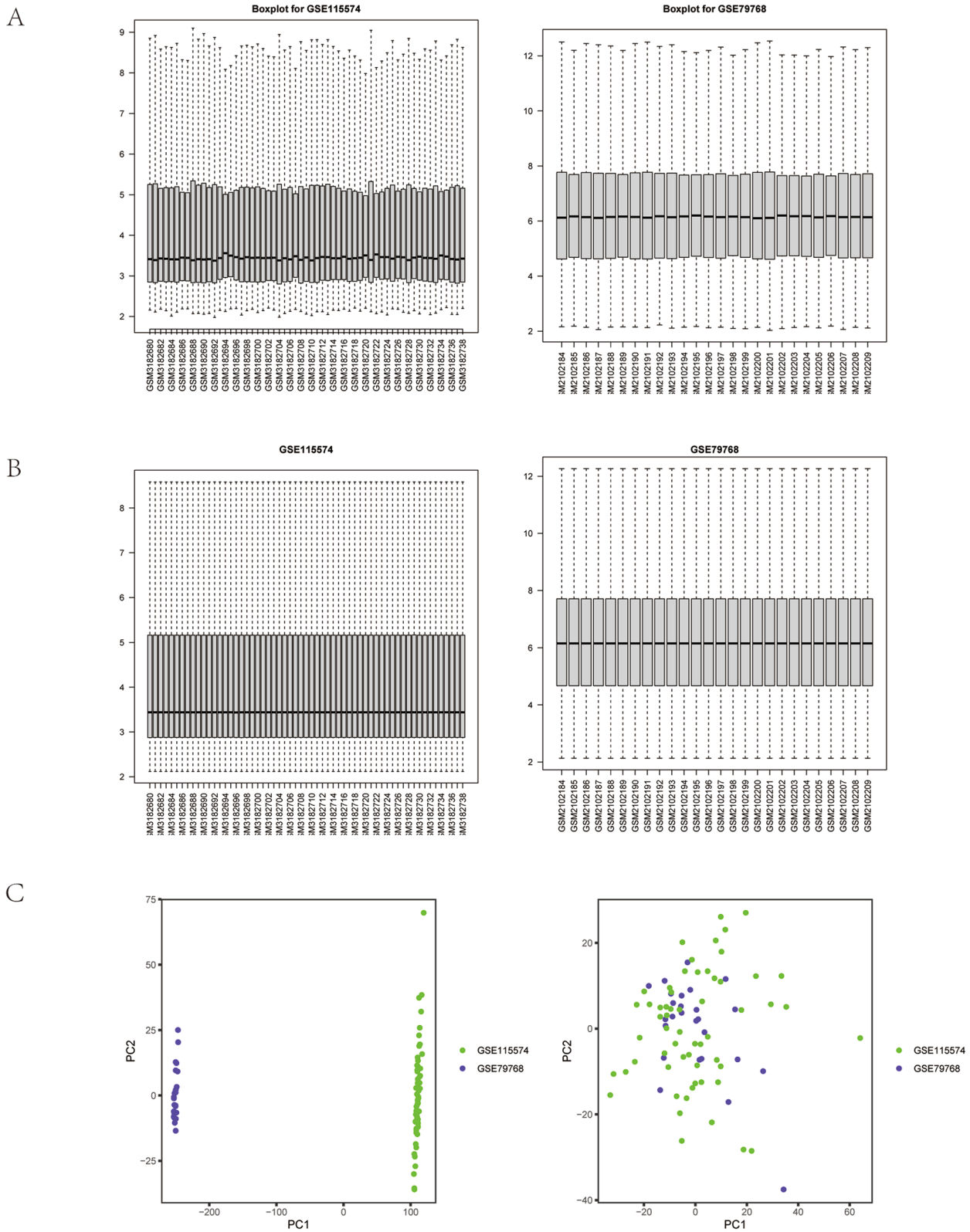

Fig. 2 The normalized expression matrices (**A-B**) and PCA plots (**C**) for the GSE115574 and GSE79768 datasets are shown. PCA, principal component analysis

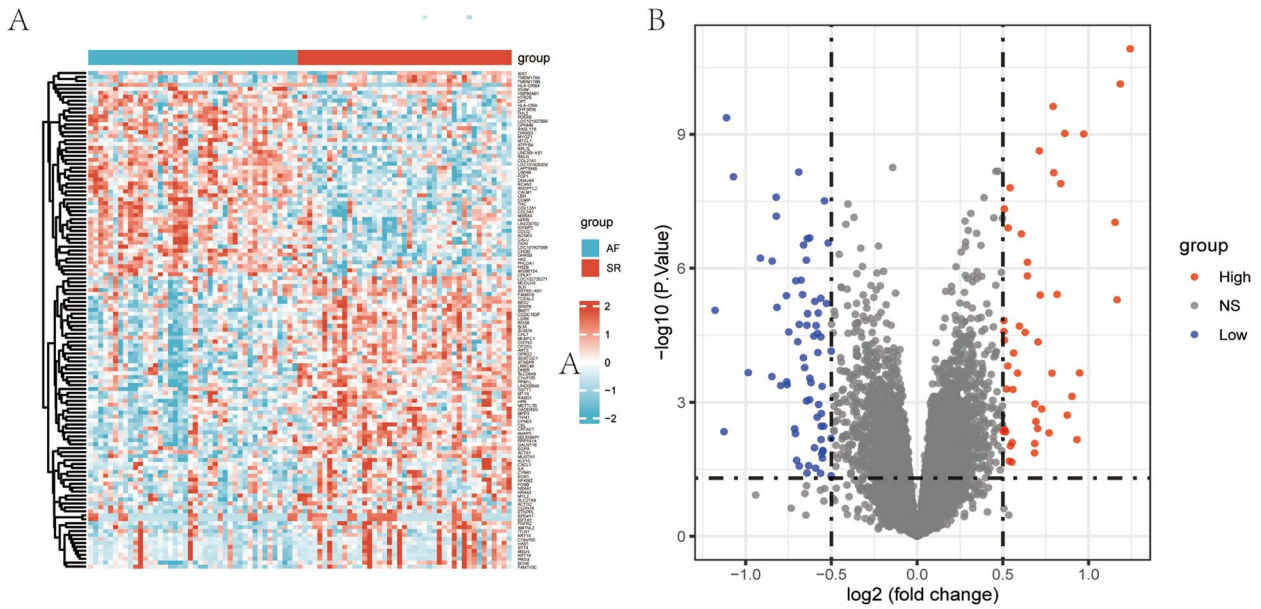

Fig. 3 **A** Heatmap visualization of the differentially expressed genes (DEGs) between atrial tissue samples from patients with atrial fibrillation (AF) and patients with sinus rhythm (SR). **B** Volcano plot visualization of the DEGs between the atrial tissue samples from patients with AF and SR, with the red and blue dots representing genes with upregulated and downregulated expression, respectively. *DEGs* differentially expressed genes, *AF* atrial fibrillation, *SR* sinus rhythm

in the Venn diagram (Fig. 4B). Remarkably, approximately one-quarter of the DEGs were predicted to be target genes of miR-450a-2-3p, highlighting the important role of this miRNA in cardiac fibrosis. GO term and KEGG pathway enrichment analyses were performed to determine the biological functions of the MRDEGs using the Metascape database. The MRDEGs were primarily associated with processes such as response to hormone, muscle tissue development, and transmembrane receptor protein serine/threonine kinase signaling pathway (Fig. 4C-D). Multiple studies have shown that the occurrence and development of atrial fibrillation are influenced by many endocrine hormones, such as thyroid hormones [9, 10]. Therefore, gland morphogenesis, especially the development of the thyroid gland, promotes the occurrence of AF. Moreover, these MRDEGs were predominantly enriched in VEGFA/VEGFR2 signaling, as shown in the network map (Fig. 4C-D). The VEGFA signaling axis promotes cardiac fibroblast proliferation and collagen synthesis and is associated with AF [11]. These findings suggest that the antifibrotic effect of miR-450a-2-3p is likely achieved through these mechanisms.

Increasing the expression of miR-450a-2-3p and inhibiting ERK(1/2) reverse cardiac fibrosis in ISO-induced mice

After demonstrating that miR-450a-2-3p targets ERK(1/2) to mediate TGF-β-induced cardiac fibrosis in vitro [8], our objective was to assess whether miR-450a-2-3p could be a potential therapeutic target for reducing cardiac fibrosis in vivo. The mice were randomly divided into four groups. The mice in the model group received intraperitoneal injections of isoproterenol (ISO), while the mice in the blank control group received an equal amount of normal saline. The mice in the experimental group and negative control group were injected with the miR-450a-2-3p agomir and agomir-NC, respectively, via the tail vein. The heart weight/body weight ratio (HW/BW) was measured in each group. The results showed an increase in HW/BW in the ISO group compared with the control group (Fig. 5A). In contrast, HW/BW was

(See figure on next page.)

Fig. 4 GO and KEGG enrichment analyses of the DEGs and MRDEGs between atrial tissue samples from patients with AF and SR. **A** Chord diagram showing the relationships between key DEGs and the most enriched GO terms. **B** Venn diagram showing the overlapping genes identified by the DEG algorithm and the predicted miR-450a-2-3p target gene algorithm. **C** Gene Ontology enrichment analysis and pathway analysis of the MRDEGs. **D** Network map including all enriched terms. The terms are colored by *p* values, with terms containing more genes tending to have a more significant p value. Enriched terms were shown in different colors. *AF* atrial fibrillation, *SR* sinus rhythm, *DEGs* differentially expressed genes, *MRDEGs* miR-450a-2-3p-related differentially expressed genes

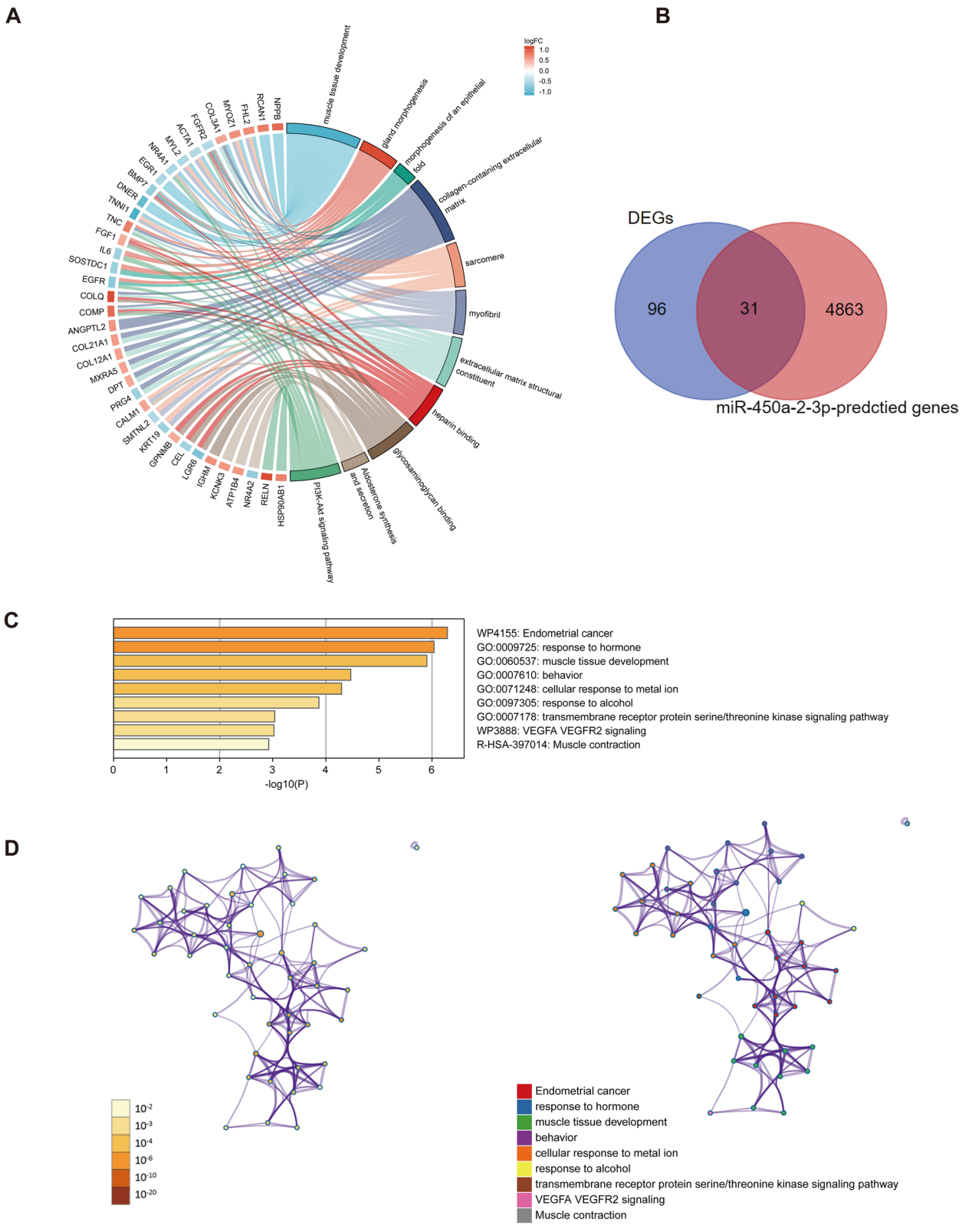

Fig. 4 (See legend on previous page.)

decreased in the ISO group after miR-450a-2-3p agonist treatment (Fig. 5A). The HE staining results suggested that compared with those in the control group, the mice in the ISO group exhibited a disordered arrangement of cardiomyocytes, and a significant increase in the number of myocardial interstitial cells (Fig. 5B). In addition, cardiomyocyte cross-sectional area statistics showed a significant increase in the cross-sectional area of cardiomyocytes in the ISO group compared to the control group (Fig. 5C). However, after injection of the miR-450a-2-3p agomir, these pathological changes improved significantly (Fig. 5B-C). Masson staining revealed collagen deposition and severe cardiac fibrosis in the ISO model group compared to the control group. However, mice injected with the miR-450a-2-3p agomir showed significant reductions in collagen deposition and the collagen volume fraction (Fig. 5B and 5D). The expression of NPPA and NPPB was detected by RT−qPCR analysis, and the results showed that the expression of NPPA and NPPB was increased in the ISO group compared with the control group. The expression of NPPA and NPPB was decreased after miR-450a-2-3p agomir treatment (Fig. 5E). These findings indicate the successful establishment of the mouse model of myocardial fibrosis at the tissue level and that miR-450a-2-3p can reverse the fibrotic process.

Furthermore, we investigated the regulatory effect of miR-450a-2-3p on fibrosis markers in mice with myocardial fibrosis. We performed RT−qPCR analysis to compare the expression level of miR-450a-2-3p in myocardial tissue between the blank control group and the ISO-induced group. Compared to that in the blank control group, the expression of miR-450a-2-3p in heart tissue in the ISO-induced group was significantly reduced. In contrast, the expression level of miR-450a-2-3p was significantly increased in the heart tissue of mice injected with the agomir, while the expression level was significantly decreased in the heart tissue in mice injected with agomir-NC. These results indicate the successful establishment of the model for the injection of the miR-450a-2-3p agonist (Fig. 5F). At the transcriptional level, overexpression of miR-450a-2-3p reduced the ISO-induced upregulation of α-SMA, COL1, and COL3 (F ig. 5G-I). The Western blot results demonstrated that the expression of these collagen biomarkers at the translational level was significantly reduced after treatment with miR-450a-2-3p, consistent with the findings at the transcriptional level. However, although COL1 expression showed a decreasing trend in the miR-450a-2-3p treatment group compared to the model group, the difference was not statistically significant (Fig. 5J-M). These findings suggest that miR-450a-2-3p inhibits ISO-induced collagen formation in heart tissue.

Similarly, to confirm whether the effect of miR-450a-2-3p on ameliorating myocardial fibrosis in mice is achieved through inhibition of ERK(1/2), we evaluated changes in the mRNA and protein expression levels of ERK(1/2) under ISO and miR-450a-2-3p intervention. The results from both the RT−qPCR and Western blot analyses demonstrated an increase in ERK(1/2) expression in the ISO-induced group, while miR-450a-2-3p treatment inhibited ERK(1/2) expression, consistent with the findings in our previous cell experiments (Fig. 5N-Q).

Discussion

AF is frequently associated with cardiac fibrosis [3]; however, the specific molecular mechanisms underlying AF remain unclear. The primary treatment methods for AF patients include drugs for rate control, oral anticoagulants for stroke prevention, antiarrhythmic drugs, and catheter ablation for conversion [12]. Despite the substantial advancements made in recent decades, the fundamental mechanisms of AF have yet to be fully understood, and effective therapies for AF are still lacking [9]. In this study, we merged two gene expression datasets from the GEO database and conducted an integrated analysis. We identified 127 DEGs and found that the processes gland morphogenesis and morphogenesis of an epithelial fold were significantly correlated with cardiac fibrosis. The occurrence and development of AF are influenced by many endocrine hormones, such as thyroid hormones. A large study indicated that among 40,628 patients diagnosed with hyperthyroidism, 3362 (8.3%) were also diagnosed with AF or flutter within ± 30 days of the hyperthyroidism diagnosis [11]. According to research data from a review, the prevalence of AF in patients with hyperthyroidism is 2%-20% [12]. Therefore, gland morphogenesis, especially the development

(See figure on next page.)

Fig. 5 Upregulation of miR-450a-2-3p attenuates the cardiac fibrosis caused by ISO. **A** Heart-to-body weight ratio ($n = 6$). **B** Pathological analysis of heart tissues from mice injected with the miR-450-a-2-3p agomir or agomir-NC was performed by HE staining and Masson staining. **C** The cross-sectional area of cardiomyocytes. **D** Collagen volume fraction (CVF). **E** The expression of NPPA and NPPB was detected by RT−qPCR. **F-I, N** The expression of miR-450a-2-3p, α-SMA, COL1, COL3 and ERK(1/2) in cardiac tissues of ISO-induced mice was measured using RT−qPCR. **J-M, O-Q** Western blot analysis was conducted to examine the expression of key regulatory proteins involved in fibrosis (α-SMA, COL1, COL3 and ERK(1/2)) in ISO-induced mice injected with the miR-450a-2-3p agomir or agomir-NC. *$P < 0.05$. **$P < 0.01$. ***$P < 0.001$. ns means no significance

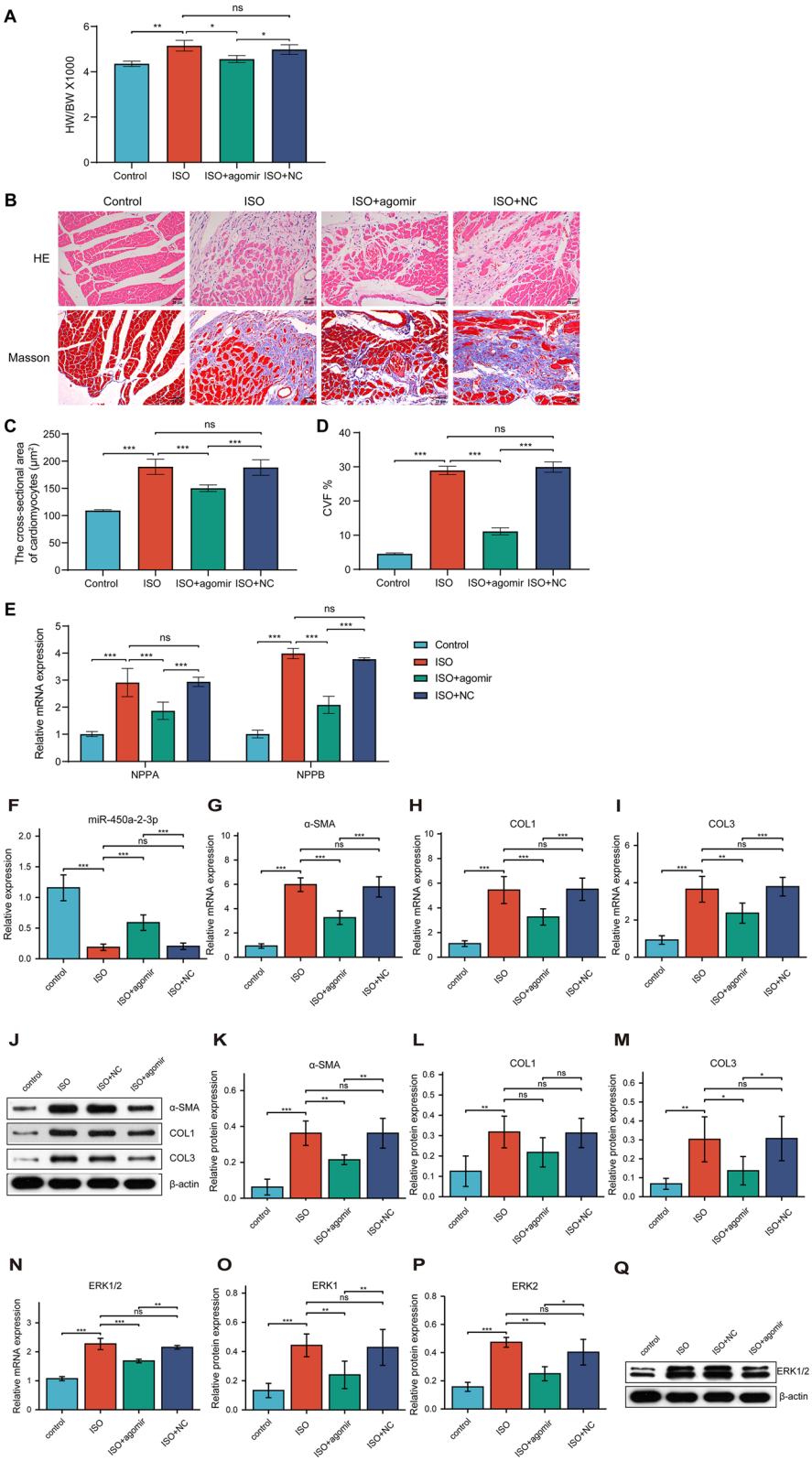

Fig. 5 (See legend on previous page.)

of the thyroid gland, promotes the occurrence of AF. The morphogenesis of an epithelial fold promotes EndMT. EndMT is a transcriptional program that downregulates the expression of endothelial genes and upregulates the expression of mesenchymal genes. Endocardial endothelial cells can transdifferentiate into fibroblasts via EndMT and contribute to extracellular matrix deposition [13–16]. Pathway analysis revealed that these 127 DEGs were strongly correlated with aldosterone synthesis and secretion and PI3K-Akt signaling. The renin–angiotensin–aldosterone system is known to play a crucial role in the structural and electrical remodeling of the heart [17]. Zhang et al. reported that the principal pathways of PI3K/AKT signaling are often activated in various pathological states, such as fibrosis, apoptosis, and regeneration after myocardial infarction [18]. Upregulated PI3K and phosphorylated AKT may be involved in the increased proliferation and migration of CFs [19].

In this study, we found that miR-450a-2-3p regulated nearly a quarter of the differentially expressed genes (DEGs). Further functional and pathway enrichment analyses based on miR-450a-2-3p were conducted using Metascape. Notably, the transmembrane receptor protein serine/threonine kinase signaling pathway, VEGFA/VEGFR2 signaling, and muscle contraction signaling pathway were identified as significantly enriched pathways. ERK(1/2), a serine/threonine kinase involved in the MAP kinase signal transduction pathway, has been reported to play a critical role in various biological processes, including myocardial fibrosis [20–23]. Guo et al. demonstrated that H19 promoted cardiac fibroblast (CF) proliferation and collagen synthesis by suppressing the miR-29a-3p/miR-29b-3p-VEGFA/TGF-β axis [11]. Furthermore, studies have suggested that the relationship between tissue factor and VEGF and its receptor in AF may indicate a possible role for VEGF in the hypercoagulable state observed in patients with AF [24]. It is evident that miR-450a-2-3p plays a crucial role in multiple functions and pathways related to cardiac fibrosis. Wu et al. reported reduced expression of miR-450a-2-3p in gastric cancer tissue, while the expression level of the oncogenic factor JHDM1D-AS1 increased. Functionally, JHDM1D-AS1 depletion caused significant reductions in cell proliferation and invasion both in vitro and in vivo, while these effects were abolished by the addition of a miR-450a-2-3p inhibitor. Mechanistically, JHDM1D-AS1 promoted gastric cancer progression by sponging miR-450a-2-3p to increase PRAF2 expression [25]. Additionally, the expression of miR-450a-2-3p was found to be reduced in a study of tuberous sclerosis complex, indicating that miR-450a-2-3p may play a crucial role in inhibiting cell proliferation [26]. However, the role of miR-450a-2-3p in myocardial fibrosis in patients with AF remains to be investigated.

Our previous findings in cardiac fibroblasts (CFs) and human umbilical vein endothelial cells (HUVECs) demonstrated that miR-450a-2-3p can suppress cardiac fibrosis by downregulating ERK(1/2) signaling [8]. In CFs, overexpression of miR-450a-2-3p attenuated the upregulation of α-SMA, COL1, and COL3 induced by TGF-β1. The CCK-8 assay revealed that TGF-β1 stimulation promoted CF proliferation but that this effect was reversed by treatment with the miR-450a-2-3p mimic. In HUVECs, TGF-β1 stimulation decreased the mRNA and protein expression levels of VE-CAD and PECAM-1/CD31 while increasing the expression levels of vimentin, COL1, and COL3. Transfection of the miR-450a-2-3p mimic reversed these changes in gene expression levels. The scratch assay demonstrated that TGF-β1 accelerated HUVEC migration, which was blocked by the miR-450a-2-3p mimic. Conversely, transfection of the miR-450a-2-3p inhibitor significantly facilitated HUVEC migration. Transfection with the miR-450a-2-3p mimic markedly reduced endogenous ERK(1/2) expression but transfection with the miR-450a-2-3p inhibitor increased ERK(1/2) mRNA and protein expression in both CFs and HUVECs. The luciferase reporter assays confirmed that miR-450a-2-3p directly targeted ERK(1/2). The overexpression of ERK(1/2) abolished the inhibitory effect of miR-450a-2-3p on CFs. Furthermore, the scratch assay showed that the inhibitory effect of the miR-450a-2-3p mimic on HUVEC migration was significantly blocked by ERK(1/2).

The aim of this study was to investigate the function and mechanism of miR-450a-2-3p in the pathogenesis of AF using a mouse model. Our data demonstrated that the overexpression of miR-450a-2-3p, a downregulated miRNA in AF [27], can alleviate cardiac fibrosis, possibly through the inhibition of ERK1/2 signaling. The first major finding of this study was the reduced expression of miR-450a-2-3p in mice treated with isoproterenol (ISO). Subsequent experiments revealed that in vivo overexpression of miR-450a-2-3p attenuated cardiac fibrosis, as evidenced by the reductions in the levels of fibrosis markers such as α-SMA, COL1, and COL3.

ERK(1/2), also known as MAPK1, belongs to the MAPK family and is involved in various cellular processes, including proliferation, differentiation, transcriptional modulation, and development. Numerous studies have demonstrated the importance of ERK(1/2) in fibrogenesis. For example, Thum et al. discovered that miR-21 modulates the ERK(1/2) signaling pathway, influencing cardiac fibroblast growth and the secretion of cytokines associated with interstitial fibrosis [22]. M. Harada et al. reported that TRPC3 regulates myocardial fibrosis progression by influencing $Ca2+$ influx through the MAPK1/miRNA-26/NFAT pathway, thereby

increasing TRPC3 expression in the myocardium [23]. Our study provides evidence for the regulatory effect of miR-450a-2-3p on ERK(1/2) in vivo.

However, it is important to acknowledge the limitations of the present study. First, we did not extensively utilize bioinformatics tools or include additional datasets to explore potential therapeutic targets. Second, our study focused solely on investigating the role of a single miRNA (miR-450a-2-3p), and future studies should aim to elucidate the functions of other potentially important miRNAs based on microarray data. Third, while our animal model successfully reproduced cardiac fibrosis in mice, it would be beneficial to conduct future studies to investigate the role of miRNAs or genes in other animal models. Last, despite the inclusion of a total of 43 (AF = 21, SR = 22) participants, the input data might still be insufficient to identify and validate key genes involved in AF development. It is worth noting that these participants were from various regions and had different diets, levels of physical activity, genetic variations, and susceptibility to cardiovascular diseases, all of which may have influenced the occurrence of AF.

Conclusion

In summary, we identified 127 differentially expressed genes (DEGs) and 31 miRNA-regulated DEGs (MRDEGs) as potential key biomarkers for AF using bioinformatics methods. Furthermore, our in vivo experiments demonstrated that the administration of miR-450a-2-3p agonist effectively attenuated isoproterenol (ISO)-induced cardiac fibrosis in mice. These findings provide insights into the molecular mechanisms underlying AF pathogenesis by elucidating the role of miR-450a-2-3p in targeting the ERK(1/2) pathway.

Abbreviations

AF	Atrial fibrillation
α-SMA	Alpha-smooth muscle actin
CFs	Cardiac fibroblasts
CVF	Collagen volume fraction
ERK (1/2)	Extracellular regulated protein kinases 1/2
HUVECs	Human umbilical vein endothelial cells
ISO	Isoproterenol
MAPK	Mitogen-activated protein kinase
MFB	Myofibroblast
RAAS	Renin-angiotensin-aldosterone system
TGF-β1	Transforming growth factor-β1

Supplementary Information

The online version contains supplementary material available at https://doi.org/10.1186/s12263-024-00753-6.

Supplementary material 1.

Acknowledgements

Not applicable.

Authors' contributions

LLS performed the experiments, conducted the data analysis, and drafted the manuscript. LFY contributed to the conception and design of the study and critically revised the manuscript. The initial draft of the manuscript was written by LLS, and all the authors provided feedback on earlier versions. All authors have read and approved the final manuscript.

Funding

This work was supported by the National Natural Science Foundation of China (no. 82070352).

Availability of data and materials

The datasets used or analyzed during the current study are available from the corresponding author upon reasonable request.

Declarations

Ethics approval and consent to participate

The study was approved by the Ethics Committee of Xiangya Hospital Central South University (201803209). The research was conducted according to the World Medical Association Declaration of Helsinki.

Competing interests

The authors declare no competing interests.

Author details

[1]Department of Emergency, The Third Xiangya Hospital of Central South University, Changsha, China. [2]Department of Cardiac Surgery, Xiangya Hospital, Central South University, Changsha, China.

Received: 5 February 2024 Accepted: 11 August 2024
Published online: 19 August 2024

References

1. Chugh SS, et al. Worldwide epidemiology of atrial fibrillation: a Global Burden of Disease 2010 Study. Circulation. 2014;129(8):837–47.
2. Cochet H, et al. Age, atrial fibrillation, and structural heart disease are the main determinants of left atrial fibrosis detected by delayed-enhanced magnetic resonance imaging in a general cardiology population. J Cardiovasc Electrophysiol. 2015;26(5):484–92.
3. Nattel S. Molecular and Cellular Mechanisms of Atrial Fibrosis in Atrial Fibrillation. JACC Clin Electrophysiol. 2017;3(5):425–35.
4. Smaill BH. Fibrosis, myofibroblasts, and atrial fibrillation. Circ Arrhythm Electrophysiol. 2015;8(2):256–7.
5. Snider P, et al. Origin of cardiac fibroblasts and the role of periostin. Circ Res. 2009;105(10):934–47.
6. Zeisberg EM, et al. Endothelial-to-mesenchymal transition contributes to cardiac fibrosis. Nat Med. 2007;13(8):952–61.
7. Prunotto M, et al. Stable incorporation of alpha-smooth muscle actin into stress fibers is dependent on specific tropomyosin isoforms. Cytoskeleton (Hoboken). 2015;72(6):257–67.
8. Liu L, Luo F, Lei K. Exosomes Containing LINC00636 Inhibit MAPK1 through the miR-450a-2-3p Overexpression in Human Pericardial Fluid and Improve Cardiac Fibrosis in Patients with Atrial Fibrillation. Mediators Inflamm. 2021;2021:9960241.
9. Nattel S, et al. Molecular Basis of Atrial Fibrillation Pathophysiology and Therapy: A Translational Perspective. Circ Res. 2020;127(1):51–72.
10. Frost L, Vestergaard P, Mosekilde L. Hyperthyroidism and risk of atrial fibrillation or flutter: a population-based study. Arch Intern Med. 2004;164(15):1675–8.
11. Guo F, et al. LncRNA H19 Drives Proliferation of Cardiac Fibroblasts and Collagen Production via Suppression of the miR-29a-3p/miR-29b-3p-VEGFA/TGF-β Axis. Mol Cells. 2022;45(3):122–33.
12. January CT, et al. 2019 AHA/ACC/HRS Focused Update of the 2014 AHA/ACC/HRS Guideline for the Management of Patients With Atrial Fibrillation: A Report of the American College of Cardiology/American Heart Association Task Force on Clinical Practice Guidelines and the Heart

Rhythm Society in Collaboration With the Society of Thoracic Surgeons. Circulation. 2019;140(2):e125–51.
13. Xu X, et al. Endocardial fibroelastosis is caused by aberrant endothelial to mesenchymal transition. Circ Res. 2015;116(5):857–66.
14. Murdoch CE, et al. Endothelial NADPH oxidase-2 promotes interstitial cardiac fibrosis and diastolic dysfunction through proinflammatory effects and endothelial-mesenchymal transition. J Am Coll Cardiol. 2014;63(24):2734–41.
15. Fan Q, et al. Twist induces epithelial-mesenchymal transition in cervical carcinogenesis by regulating the TGF-beta/Smad3 signaling pathway. Oncol Rep. 2015;34(4):1787–94.
16. Piera-Velazquez S, Jimenez SA. Endothelial to Mesenchymal Transition: Role in Physiology and in the Pathogenesis of Human Diseases. Physiol Rev. 2019;99(2):1281–324.
17. Iraqi W, et al. Extracellular cardiac matrix biomarkers in patients with acute myocardial infarction complicated by left ventricular dysfunction and heart failure: insights from the Eplerenone Post-Acute Myocardial Infarction Heart Failure Efficacy and Survival Study (EPHESUS) study. Circulation. 2009;119(18):2471–9.
18. Zhang Q, et al. Signaling pathways and targeted therapy for myocardial infarction. Signal Transduct Target Ther. 2022;7(1):78.
19. Yang W, et al. BMI1 promotes cardiac fibrosis in ischemia-induced heart failure via the PTEN-PI3K/Akt-mTOR signaling pathway. Am J Physiol Heart Circ Physiol. 2019;316(1):H61–9.
20. Davis J, et al. A TRPC6-dependent pathway for myofibroblast transdifferentiation and wound healing in vivo. Dev Cell. 2012;23(4):705–15.
21. Han L, Li J. Canonical transient receptor potential 3 channels in atrial fibrillation. Eur J Pharmacol. 2018;837:1–7.
22. Thum T, et al. MicroRNA-21 contributes to myocardial disease by stimulating MAP kinase signalling in fibroblasts. Nature. 2008;456(7224):980–4.
23. Harada M, et al. Transient receptor potential canonical-3 channel-dependent fibroblast regulation in atrial fibrillation. Circulation. 2012;126(17):2051–64.
24. Chung NA, et al. Is the hypercoagulable state in atrial fibrillation mediated by vascular endothelial growth factor? Stroke. 2002;33(9):2187–91.
25. Wu M, et al. JHDM1D-AS1 aggravates the development of gastric cancer through miR-450a-2-3p-PRAF2 axis. Life Sci. 2021;265.
26. Cai Y, et al. MicroRNA differential expression profile in tuberous sclerosis complex cell line TSC2(-/-) MEFs and normal cell line TSC2(+/+) MEFs. Beijing Da Xue Xue Bao Yi Xue Ban. 2017;49(4):580–4.
27. Liu L, et al. Identification of microRNAs enriched in exosomes in human pericardial fluid of patients with atrial fibrillation based on bioinformatic analysis. J Thorac Dis. 2020;12(10):5617–27.

Publisher's Note